Thin–Walled Structures 161 (2021) 107475

Contents lists available at ScienceDirect

Thin-Walled Structures

journal homepage: www.elsevier.com/locate/tws

Full length article

Load-bearing capacity of cold-formed sinusoidal steel sheets

Marsel Garifullin [a,*], Kristo Mela [a], Thibault Renaux [b], David Izabel [c], Rainer Holz [d], Christian Fauth [e]

[a] Tampere University, Korkeakoulunkatu 10, 33720 Tampere, Finland
[b] Joris Ide, Hille 174, 8750 Zwevezele, Belgium
[c] L'Enveloppe Métallique du Bâtiment, rue La Pérouse 6-14, 75784 Paris, France
[d] Ingenieurbüro für Leichtbau, Rehbuckel 7, 76228 Karlsruhe, Germany
[e] Karlsruhe Institute of Technology, Otto-Ammann-Platz 1, 76131 Karlsruhe, Germany

ARTICLE INFO

Keywords:
Cold-formed structures
Sinusoidal sheet
Load-bearing capacity
Multi-span sheeting
Experiment

ABSTRACT

Currently, corrugated cold-formed steel sheets are widely used as parts of cladding panels and roof envelopes in public and residential buildings. However, the design of corrugated sheets is weakly covered by the current building codes. This paper investigates the load-bearing capacity of corrugated steel sheets with the sinusoidal profile, presenting the results of the experimental research that was performed in the GRISPE project at the Research Center for Steel, Timber and Masonry, Karlsruhe Institute of Technology (KIT). Three types of tests were carried out: (1) single span tests under downward loading, (2) internal support tests under downward and upward loading to investigate the moment-support interaction and (3) end support tests under downward loading to determine the local resistance of the profiles. The obtained results are used to validate the design methods for bending moment resistance of sinusoidal sheets. The validation demonstrated that the conventional design method and the Swedish code for light-gauge structures StBK-N5 provide a safe and accurate prediction of the resistance and can be recommended as simple design rules for sinusoidal sheets. The Eurocode for silos, EN 1993-4-1:2007, was found to provide a simplified solution for calculating the section properties of the sinusoidal profile. In addition, the obtained experimental results showed that internal supports can considerably reduce the bending moment capacity in the span of the sheet. Some conclusions are made on the dependency of M/R-interaction on the direction of loading, the fixing type and the support width.

1. Introduction

Corrugated steel sheets represent one of the oldest cold-formed steel sheets used in cladding panels and roofing envelopes. Usually, corrugated sheets have flat trapezoidal or sinusoidal profiles. Sinusoidal sheets have a continuous curvature, as demonstrated in Fig. 1a. Currently, sinusoidal sheets are effectively used in public (Fig. 2a) and residential buildings (Fig. 2b). Usually, industrial sinusoidal profiles are fastened in the crest or in the valley, as shown in Fig. 1b.

The bending resistance of corrugated sheeting represents quite a complicated issue. The design code for cold-formed structures, EN-1993-1-3:2006 [1], does not cover the design of corrugated steel sheets. Comprehensive research on the inelastic flexural stability of sinusoidal sheets was conducted by Wakeland [2] and Cary [3]. The properties of corrugated profiles were later investigated in [4–10]. The paper [11] explores the strength of corrugated sheets under cyclic wind loading. In addition, a great deal of publications investigate corrugated sheets as a part of sandwich panels [12,13], shear walls [14–18] or beams with a sinusoidal web [19–22].

The bending moment capacity of trapezoidal sheeting is investigated in [23,24]. Le Tran et al. [25] presented a calculation method that considers the usual procedure for buckling problems and proposes parameters developed from the comparison with finite element calculations.

Generally, the failure of corrugated profiles in bending occurs through plastic deformation with no local buckling because of the small slenderness. The failure under local loads occurs through plastic deformation of the crests or valleys of the profile.

The existing design methods allow to calculate the design resistance M_{Rd} of sinusoidal sheets on two supports (single span bending). However, the corrugated sheets employed in roofing systems usually have several spans. In such cases, the behavior of sheets is also influenced by the support reactions that appear close to internal supports. The support reactions lead to local deformations of the cross-section and shear

* Corresponding author.
E-mail address: marsel.garifullin@tuni.fi (M. Garifullin).

https://doi.org/10.1016/j.tws.2021.107475
Received 14 April 2020; Received in revised form 12 January 2021; Accepted 15 January 2021
Available online 27 January 2021

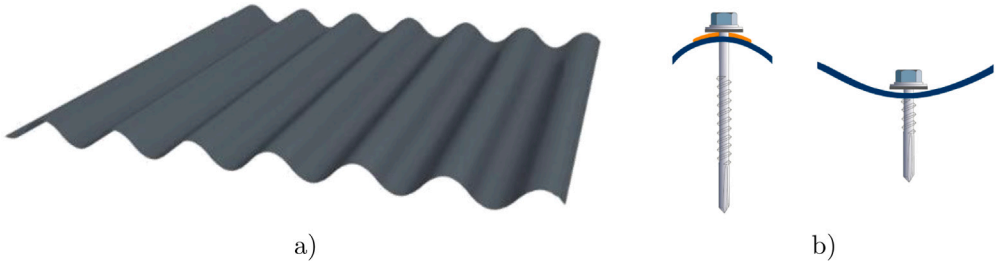

Fig. 1. Sinusoidal sheet: (a) overall view; (b) fastening of the sheet in the crest (left) and in the valley (right).

Fig. 2. Application of sinusoidal profiles: (a) SNC Pont d'Ouit (Architect: DGA-Architecture); (b) Aiguillon Construction (Architect: Christophe Rousselle Architecte).

stresses, which can considerably reduce the bending moment capacity of the sheet. Therefore, the failure of the sheet often occurs from a local failure in the support or from an interaction between the bending moment and the support reaction. Currently, none of the presented design approaches considers these two phenomena for sinusoidal sheets and this problem remains unsolved.

To fulfill this gap, this paper presents experimental research on cold-formed sheets with sinusoidal profiles, which was conducted in the framework of the GRISPE project. Three types of tests were conducted according to Annex A.2 of EN 1993-1-3:2006 [1]: single span tests, internal support tests (under downward and upward loading) and end-support tests (including shear tests). The single span tests were performed to investigate the load-bearing capacity of sinusoidal sheets under single span bending. The obtained results are used to validate the existing design methods for sinusoidal sheets. The internal support tests were conducted to explore the behavior of sheets under the combination of bending and the support reaction and investigate their M/R-interactions. End support tests were performed to analyze the behavior of sinusoidal sheets under local loads, i.e. end support resistance.

Fig. 3 provides the cross-section of the sinusoidal sheet together with its geometrical parameters. This paper employs the notations of EN 1993-4-1:2007, where t is the thickness of the sheet, l is the wavelength of the corrugation, d is the crest to crest dimension and R_ϕ is the local radius at the crest or trough.

2. Existing methods for the design of sinusoidal sheeting

As this paper employs as much as possible the current design procedures, this section presents a short state-of-the-art of the existing methods to calculate the resistance of sinusoidal sheets.

2.1. Conventional design method

The conventional design method starts from the calculation of the section modulus W_y per width of the cross-section of the sheet. The section modulus can be found assuming either elastic ($W_{el,y}$) or plastic ($W_{pl,y}$) distribution of stresses in the cross-section. In particular, the elastic section modulus per unit width can be calculated from the second moment of area I_y:

$$W_{el,y} = \frac{I_y}{d/2} \tag{1}$$

The calculation of the exact second moment of area I_y of the sinusoidal profile requires the consideration of the arc-and-tangent thin-walled line according to the equations from Strength of Materials or, if available, some software. For this reason, the calculation procedure might be very complicated, particularly for engineering purposes. An alternative solution for obtaining section properties can be found in the Eurocode standard for silos, EN 1993-4-1:2007 [26]. Although this standard is not generally applicable for the design of sinusoidal sheets, it contains very simple equations to calculate the section properties of sinusoidal profiles. In particular, the second moment of area per unit width can be calculated as

$$I_y = 0.13td^2 \tag{2}$$

Using Eq. (2), the elastic section modulus can be found as

$$W_{el,y} = 0.26td \tag{3}$$

In this paper, the alternative equation will be analyzed in addition to the exact approach from the Strength of Materials. The accuracy and validity range of the alternative approach will be specified.

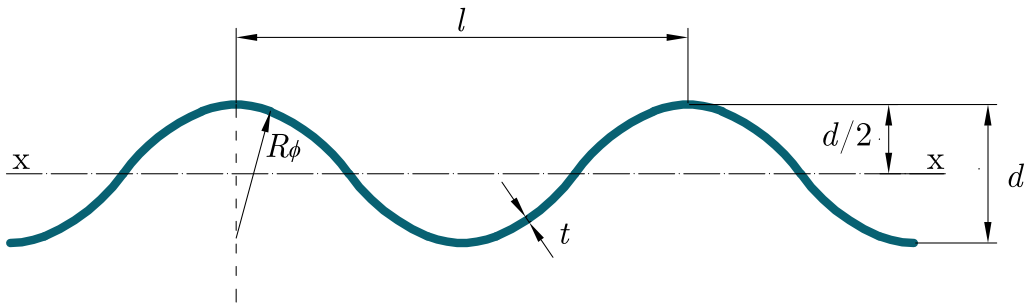

Fig. 3. Geometrical parameters of sinusoidal sheet.

When the section modulus of the sinusoidal sheet is known, the characteristic moment resistance can be found as

$$M_{c,Rd} = \frac{W_y f_{yb}}{\gamma_{M0}} \tag{4}$$

where f_{yb} is the yield strength of the sheet.

2.2. Design according to StBK-N5

The Swedish code for light-gauge metal structures StBK-N5 [27] allows to determine the ultimate bending moment for corrugated profiles with sinusoidal or similar cross-sections considering the local buckling phenomenon. The calculation procedure depends on the R_ϕ/t ratio. If $R_\phi/t \le 0.04E/f_{yb}$, there is no need to check the cross-section for the local buckling and the bending moment resistance is determined as in Section 2.1, i.e. $M_{c,Rk} = W_y f_{yb}$. Here E is the Young's modulus of steel. If $R_\phi/t > 0.04E/f_{yb}$, the moment resistance is calculated using reduced compressive stress, which can be calculated by the following steps:

1. Coefficient η:

$$\eta = 0.19 + 0.67/\sqrt{1 + R_\phi/(100t)} \tag{5}$$

2. Reduced buckling stress:

$$\sigma_{elr} = 0.60\eta Et/R_\phi \tag{6}$$

3. Slenderness ratio:

$$\alpha = \sqrt{f_{yb}/\sigma_{elr}} \tag{7}$$

4. Reduced compressive stress:

$$\sigma_c = \begin{cases} f_{yb}, & \alpha \le 0.30 \\ (1.126 - 0.419\alpha)\cdot f_{yb}, & 0.30 < \alpha \le 1.10 \\ 0.8/\alpha^2 \cdot f_{yb}, & 1.10 < \alpha \end{cases} \tag{8}$$

5. Bending moment:

$$M_{c,Rk} = W_y \sigma_c \tag{9}$$

In the serviceability limit state, the moment of inertia should be calculated with the stress reduced to $\sigma_c = f_{yb}/1.5$.

3. Experimental study

The tests were performed at the Research Center for Steel, Timber and Masonry, Karlsruhe Institute of Technology (KIT). Two mostly used sinusoidal steel profiles were selected for the tests: a small corrugated steel sheet, Sin-18/76, and a large corrugated steel sheet, Sin-46/150. The profiles are current representatives in the building market in terms of geometry. Both profiles were analyzed with two nominal thicknesses t_{nom} of 0.63 mm and 1.00 mm. The geometry and the thicknesses of the profiles were selected in such a way as to investigate different failure modes of the sheets: the profiles with small corrugations and large thickness were expected to fail from yielding, while buckling was expected for the profiles with large corrugations and small thickness. For the profiles with intermediate properties, a combination of failure modes was expected.

Table 1
Properties of the tested profiles.

Profile	d [mm]	l [mm]	R_ϕ [mm]	b_v [mm]	t_{nom} [mm]	R_ϕ/t	q [kN/m^2]
Sin-18/76	18	76	23	456	0.63	36.5	0.063
					1.00	23.0	0.099
Sin-46/150	46	150	30	900	0.63	47.6	0.067
					1.00	30.0	0.106

The steel sheets were made of S320GD steel according to EN 10346:2015 [28], with the yield stress f_{yb} = 320 MPa and the ultimate stress f_u = 390 MPa. On both sides, the sheets were covered by a zinc layer. Table 1 presents the dimensions of the analyzed profiles in accordance with Fig. 3, as well as their width b_v, R_ϕ/t-ratio and self-weight q.

Three types of tests were carried out:

1. single span tests with a positive bending moment (downward loading),
2. internal support tests for the moment-support interaction with downward and upward loading,
3. end support tests and shear tests with downward loading.

The configuration of all the conducted tests followed the recommendations of EN 1993-1-3:2006 [1, Annex A.2]. The experimental program is presented separately for every type of tests and includes the tests with varying sheet thicknesses t_{nom}, support widths b_u and spans L. The spans were chosen such that the test results could represent the moment resistance of the sheet. To reduce measurement errors, each configuration of the tests was repeated at least two times, except the shear tests.

To determine the actual material properties, tensile tests were performed on the specimens according to ISO 6892-1:2009 [29]. Three specimens per sheet and per thickness were cut from the steel coils that were used to produce the sheets. The yield strength $f_{yb,obs}$ and the tensile strength $f_{ub,obs}$ were determined based on the measured steel core thickness $t_{cor,obs}$. The results of the tensile tests are collected in Table 2, where A_{80} denotes the elongation at fracture (on 80 mm basis). As can be seen, the scattering of the individual values among the samples of the same coil was very small; therefore, the mean values were employed as representatives for all the conducted tests.

3.1. Single span tests

The single span tests were performed under downward loading. The uniformly distributed load was simulated by four point loads, as demonstrated in Fig. 4. Due to the isostatic load distribution, all the four loads were equal. The load was applied to the valleys of the sheets through transverse timber beams with the width of no less than $1.4d$.

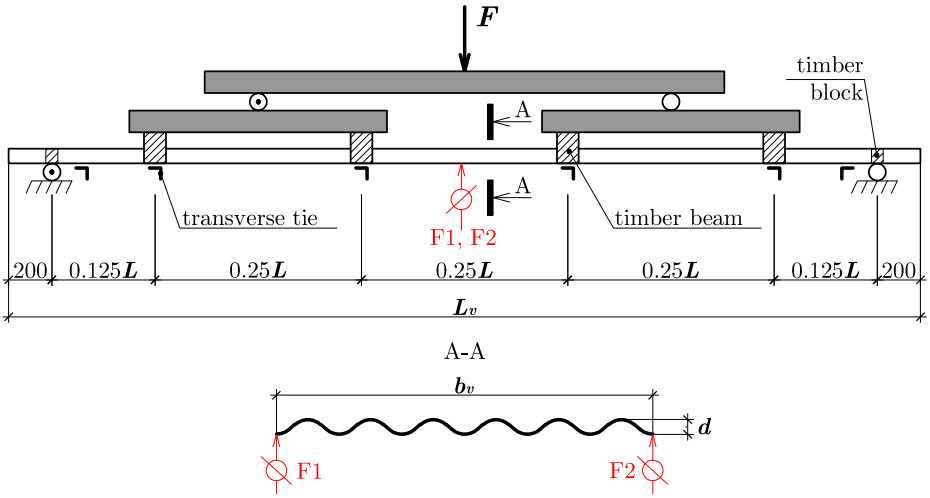

Fig. 4. Test setup for single span tests. Dimensions in [mm].

Table 2
Measured material properties.

Profile	t_{nom} [mm]	Test No.	$t_{cor,obs}$ [mm]	$f_{yb,obs}$ [MPa]	$f_{ub,obs}$ [MPa]	A_{80} [%]
Sin-18/76	0.63	1	0.50	339	469	24.6
		2	0.55	340	462	25.3
		3	0.52	322	450	24.8
		mean	0.523	333.7	460.3	24.9
	1.00	1	0.93	404	458	20.9
		2	0.96	412	457	21.7
		3	0.94	390	453	22.0
		mean	0.943	402.0	456.0	21.5
Sin-46/150	0.63	1	0.51	361	409	28.5
		2	0.53	362	410	28.9
		3	0.52	370	409	27.4
		mean	0.520	364.3	409.3	28.3
	1.00	1	0.92	413	462	21.2
		2	0.95	422	465	21.7
		3	0.93	392	457	21.8
		mean	0.933	409.0	461.3	21.6

Timber blocks with the width of 50 mm were used to avoid local deformations at the end supports. Angular transverse ties were used to prevent the profiles from spreading. The deflections were measured in the middle of the span by two trip wire displacement sensors, F1 and F2, located under the bottom flanges. The loading was performed by a load cell with a maximum capacity of 50 kN. At the beginning of the loading, a preload F_{pr} was implied to cover possible gaps in the experimental setup. The deflection-controlled load was applied and measured with a speed of 30 mm/min.

The experimental program for the single span tests is presented in Table 3, with the specimens named in the manner `SSP-AA-BBB-C`, where

`SSP` is "Single Span Positive bending test";
`AA` is the profile height, d [mm];
`BBB` is the nominal sheet thickness, $t_{nom} \times 100$ [mm];
`C` is the test number.

The test setup for the test SSP-18-100-1 is illustrated in Fig. 5.

3.2. Internal support tests

The internal support tests were performed under downward and upward loading. The procedure, nomenclature and terminology used in these tests are consistent with the CSTB standard for deck profiles [30] and EN-1993-1-3:2006 [1]. For downward loading, the load was applied in the middle of the span through a transverse steel beam with a width of b_u = 10 mm or b_u = 40 mm, as demonstrated in Figs. 6 and 7a. For upward loading, the load was applied through M6 bolts and d = 16 mm washers to each valley or crest of the sheets, as shown in Figs. 8 and 7b. The length of all specimens was L_v = 1500 mm. Angular

Fig. 5. Single span tests: SSP-18-100-1.

Table 3
Single span tests: experimental program.

Test	Profile	t_{nom} [mm]	L [mm]	L_v [mm]	b_v [mm]	F_{pr} [kN]
SSP-18-063–1 SSP-18-063–2 SSP-18-063–3	Sin-18/76	0.63	1500	1900	456	0.25
SSP-18-100–1 SSP-18-100–2 SSP-18-100–3	Sin-18/76	1.00	2000	2400	456	0.26
SSP-46-063–1 SSP-46-063–2 SSP-46-063–3 SSP-46-063–4 SSP-46-063–5 SSP-46-063–6	Sin-46/150	0.63	2000	2400	900	0.22
SSP-46-100–1 SSP-46-100–2 SSP-46-100–3	Sin-46/150	1.00	3000	3400	900	0.51

Table 4
Internal support tests: experimental program.

Downward loading									
Test	L [mm]	b_u [mm]	t_{nom} [mm]	Profile	Test	L [mm]	b_u [mm]	t_{nom} [mm]	Profile
IS-18-10-063-40–1 IS-18-10-063-40–2	400	10	0.63	Sin-18/76	IS-46-10-063-60–1 IS-46-10-063-60–2	600	10	0.63	Sin-46/150
IS-18-10-063-80–1 IS-18-10-063-80–2	800				IS-46-10-063-100–1 IS-46-10-063-100–2	1000			
IS-18-40-063-40–1 IS-18-40-063-40–2	400	40			IS-46-40-063-60–1 IS-46-40-063-60–2	600	40		
IS-18-40-063-80–1 IS-18-40-063-80–2	800				IS-46-40-063-100–1 IS-46-40-063-100–2	1000			
IS-18-10-100-40–1 IS-18-10-100-40–2	400	10	1.00	Sin-18/76	IS-46-10-100-60–1 IS-46-10-100-60–2	600	10	1.00	Sin-46/150
IS-18-10-100-100–1 IS-18-10-100-100–2	1000				IS-46-10-100-120–1 IS-46-10-100-120–2	1200			
IS-18-40-100-40–1 IS-18-40-100-40–2	400	40			IS-46-40-100-60–1 IS-46-40-100-60–2	600	40		
IS-18-40-100-100–1 IS-18-40-100-100–2	1000				IS-46-40-100-120–1 IS-46-40-100-120–2	1200			
Upward loading									
Test	L [mm]	Fixing	t_{nom} [mm]	Profile	Test	L [mm]	Fixing	t_{nom} [mm]	Profile
IS-18-V-063-40–1 IS-18-V-063-40–2	400	Valley	0.63	Sin-18/76	IS-46-V-063-60–1 IS-46-V-063-60–2	600	Valley	0.63	Sin-46/150
IS-18-V-063-80–1 IS-18-V-063-80–2	800				IS-46-V-063-100–1 IS-46-V-063-100–2	1000			
IS-18-C-063-40–1 IS-18-C-063-40–2	400	Crest			IS-46-C-063-60–1 IS-46-C-063-60–2	600	Crest		
IS-18-C-063-80–1 IS-18-C-063-80–2	800				IS-46-C-063-100–1 IS-46-C-063-100–2	1000			
IS-18-V-100-40–1 IS-18-V-100-40–2	400	Valley	1.00	Sin-18/76	IS-46-V-100-90–1 IS-46-V-100-90–2	600	Valley	1.00	Sin-46/150
IS-18-V-100-100–1 IS-18-V-100-100–2	1000				IS-46-V-100-140–1 IS-46-V-100-140–2	1200			
IS-18-C-100-40–1 IS-18-C-100-40–2	400	Crest			IS-46-C-100-90–1 IS-46-C-100-90–2	600	Crest		
IS-18-C-100-100–1 IS-18-C-100-100–2	1000				IS-46-C-100-140–1 IS-46-C-100-140–2	1200			

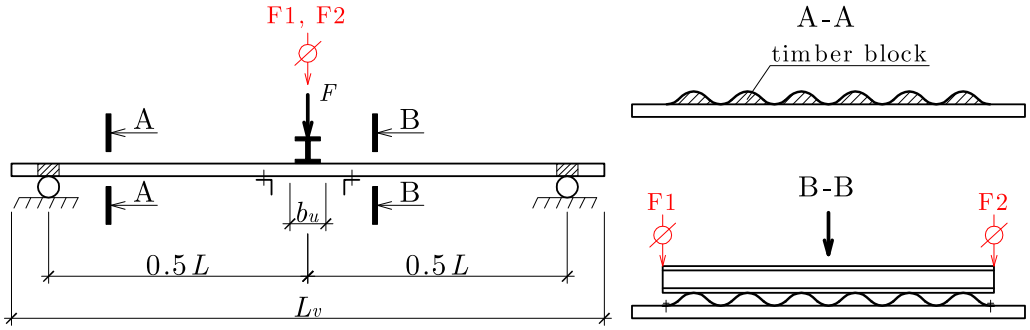

Fig. 6. Test setup for internal support tests, downward loading.

transverse ties were used to prevent the profiles from spreading. Timber blocks were used to avoid local deformations at the end supports.

The deflections were measured continuously by two trip wire displacement sensors, F1 and F2, located in the middle of the span at the transverse beam. At the beginning of the loading, a preload F_{pr} was implied to cover possible gaps in the experimental setup. For Sin-18/76, the magnitude of the preload was equal to 0.03 kN in both downward and upward loading. For Sin-46/150, the magnitude of the preload was equal to 0.06 kN and 0.24 kN in downward and upward loading, respectively. The deflection-controlled load was applied and measured with a speed of 3–6 mm/min. After a maximum load was reached, the loading speed was increased to 10 mm/min. The experimental program for the internal span tests is presented in Table 4, with the specimens named in the manner `IS-AA-BB-CCC-DDD-E`, where

`IS`	is “Internal Support tests”;
`AA`	is the profile height, d [mm];
`BB`	is the support width b_u [mm] for downward loading or the fastening type for upward loading (V for valley and C for crest);
`CCC`	is the nominal sheet thickness, $t_{nom} \times 100$ [mm];
`DDD`	is the span length, L [cm];
`E`	is the test number.

Fig. 7. Internal support tests: (a) downward loading; (b) upward loading.

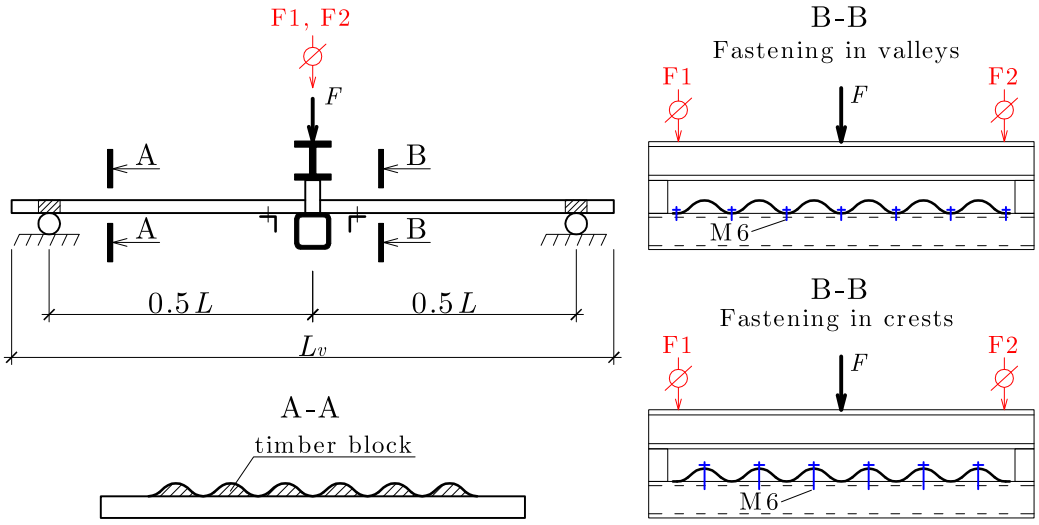

Fig. 8. Test setup for internal support tests, upward loading.

3.3. End support tests and shear tests

The end support and shear tests were performed under downward loading to determine the end support resistance. The test setup is demonstrated in Fig. 9. The length of all sheets was L_v = 1500 mm. The load was applied by a transverse steel plate with the width of b. The profiles were prevented from spreading by transverse ties. In the end support tests, the analyzed support represented a beam with a cutting edge (gradient 1:20). In the shear tests, the analyzed support represented a timber block with no cutting edge. At the opposite end support, timber blocks were used to avoid web crippling in all the tests. The deflections were measured continuously by two trip wire displacement sensors, F1 and F2, located on the crests of the sheets above the analyzed end support. At the beginning of the loading, a preload F_{pr} was implied to cover possible gaps in the experimental setup. The deflection-controlled load was applied with a speed of 3 mm/min and was measured continuously using a calibrated load cell. The experimental program for the end support and shear tests is presented in Table 5, with the specimens named in the manner A-BB-CCC-DDD-E, where

A	is "End Support test" (ES-Q) or "Shear test" (S);
BB	is the profile height, d [mm];
CCC	is the nominal sheet thickness, $t_{nom} \times 100$ [mm];
DDD	is the span length, L [cm];
E	is the test number.

The test setup for the test ES-Q-46-063-105-1 is illustrated in Fig. 10.

4. Results

This section presents and discusses the results of all the three types of tests. The characteristic values for all the tests are obtained conducting the statistical treatment according to EN 1993-1-3:2006 [1, Annex A.6.3] considering families of tests. In this paper, a test series represents a combination of the profile type, boundary conditions and sheet thickness, e.g. SSP-18-063-1 to SSP-18-063-3. A series of test series represents all the test series of the same test type, e.g. all single span tests (SSP-...). These test series are evaluated together, i.e. the standard deviation is determined from the total amount of tests, e.g. n = 15 for the single-span tests. Each test result is set in relation to the mean value of the test series, and the standard deviation s is calculated from the quotient. The characteristic values for each test series are then calculated with the resulting standard deviation s and the k-factor according to [1, Table A.2].

4.1. Single span tests

All single span tests demonstrated a linear load–deflection behavior almost until the failure, as can be seen in Figs. 11 and 12. In the figures, F_{max} indicates the failure load, i.e. the maximum load the specimen resisted. The deviations between the values of the displacements F1

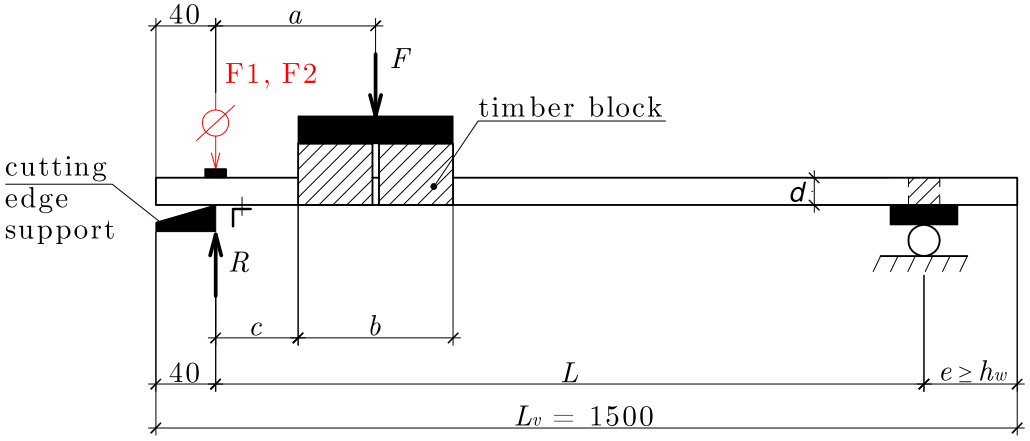

Fig. 9. Test setup for end support tests and shear tests. Dimensions in [mm].

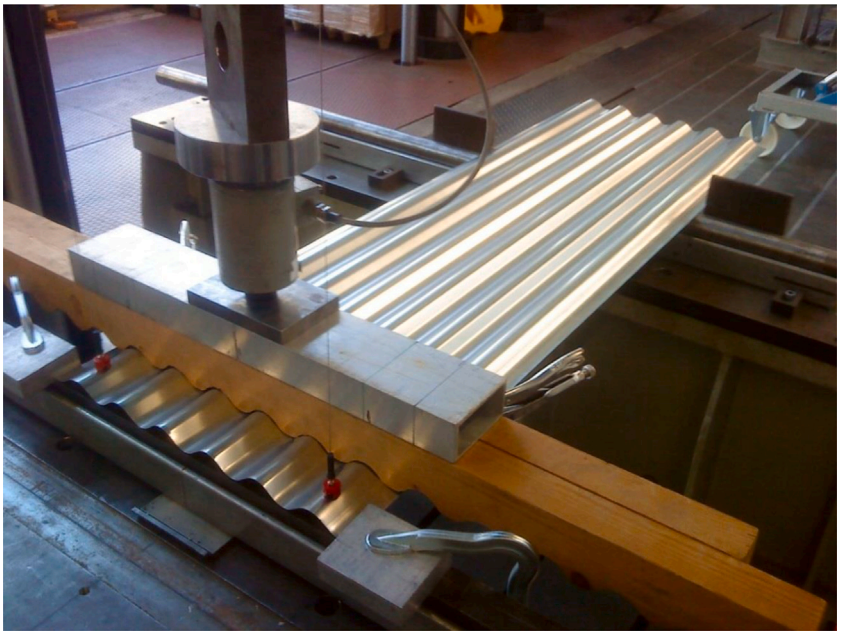

Fig. 10. End support tests and shear tests: ES-Q-46-063-105-1.

and F2 in the subcritical range (before reaching F_{max}) were mostly negligible; therefore, the displacements F1 and F2 are shown by a common curve. For the profile Sin-18/76 with t_{nom} = 1.00 mm, the failure occurred by a plastic deformation along the whole span of the sheets, as shown in Fig. 13a. In all other tests, the failure occurred by buckling of crests in the middle of the span, as depicted in Fig. 13b. The results of the single span tests are listed in Table 6.

Based on the similarity of the conducted tests, the two profiles were combined into one test family, assuming that both profiles belong to the same population. The k-factor was chosen equal to 1.92, corresponding to a sample size of $n \geq 10$ (actual number of single span tests n = 15) with unknown V_x according to [1, Table A.2]. The characteristic bending moment in the span was calculated by the following equation:

$$M_{c,Rk,F} = \frac{F_{u,k} L}{8 b_v} + \frac{q L_v (2L - L_v)}{8} \tag{10}$$

where $F_{u,k}$ is the characteristic load (including preload); L, L_v and b_v are the span, length and width of the sheet, respectively (Fig. 4); q is the self-weight of the sheet (Table 1). The characteristic bending moments for the tested profiles after the statistical treatment are summarized in Table 6.

Table 5
End support tests and shear test: experimental program.

Test	Profile	t_{nom} [mm]	a [mm]	b [mm]	c [mm]	L [mm]	b_v [mm]	F_{pr} [kN]
ES-Q-18-063-100–1 ES-Q-18-063-100–2 ES-Q-18-063-100–3	Sin-18/76	0.63	100	100	50	1000	456	0.09
ES-Q-18-100-100–2 ES-Q-18-100-100–3 ES-Q-18-100-100–4	Sin-18/76	1.00	100	100	50	1000	456	0.09
ES-Q-46-063-105–1 ES-Q-46-063-105–2 ES-Q-46-063-105–3	Sin-46/150	0.63	150	100	100	1050	900	0.10
ES-Q-46-100-105–1 ES-Q-46-100-105–2 ES-Q-46-100-105–3	Sin-46/150	1.00	150	100	100	1050	900	0.10
S-18-063-100–1	Sin-18/76	0.63	80	100	30	1000	456	0.06
S-46-063-100–1	Sin-46/150	0.63	115	100	70	1000	900	0.06

Using the obtained experimental results, the paper validates the above-mentioned methods (Section 2) for the calculation of the bending

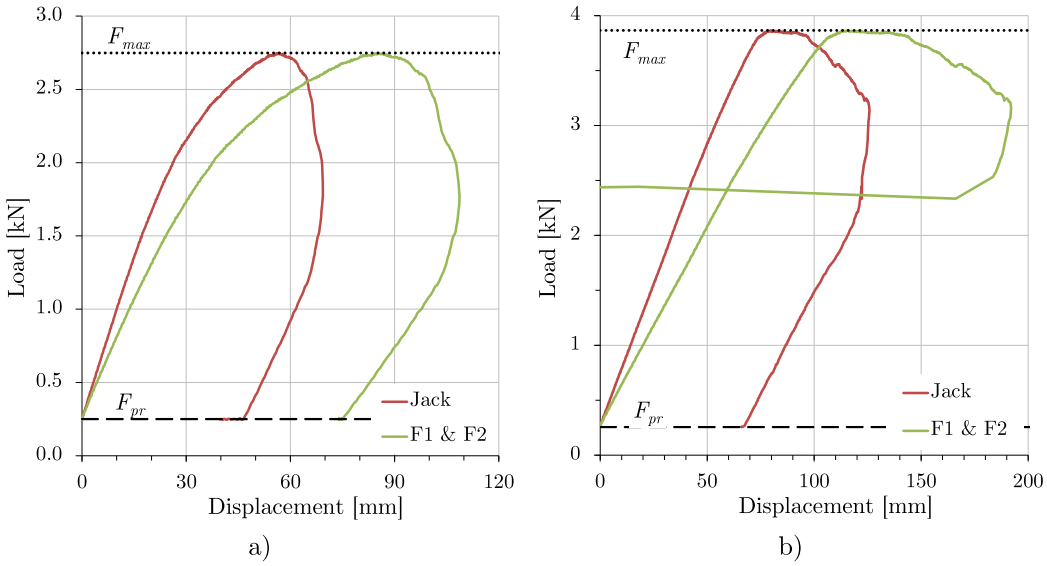

Fig. 11. Load–deflection curves: (a) SSP-18-063-1; (b) SSP-18-100-1.

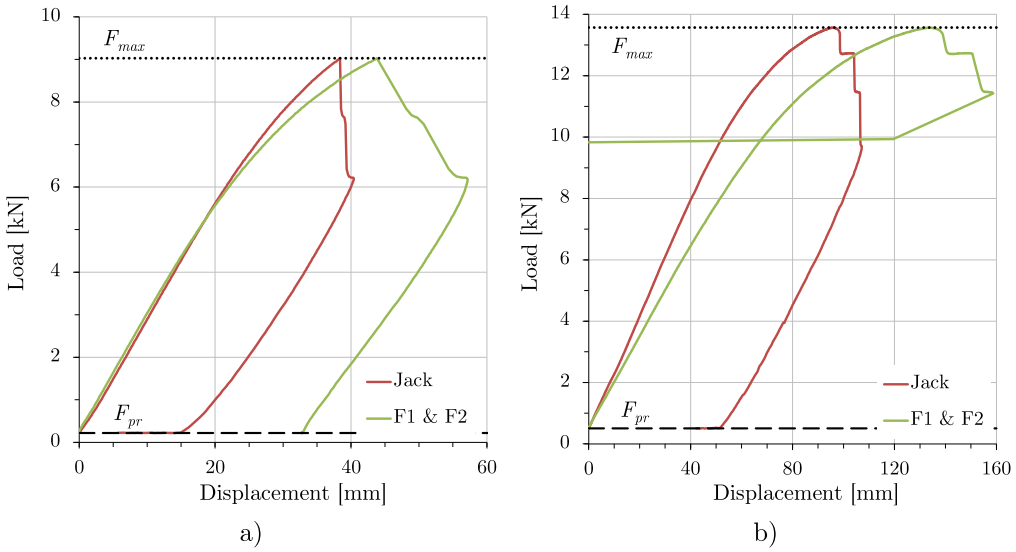

Fig. 12. Load–deflection curves: (a) SSP-46-063-2; (b) SSP-46-100-1.

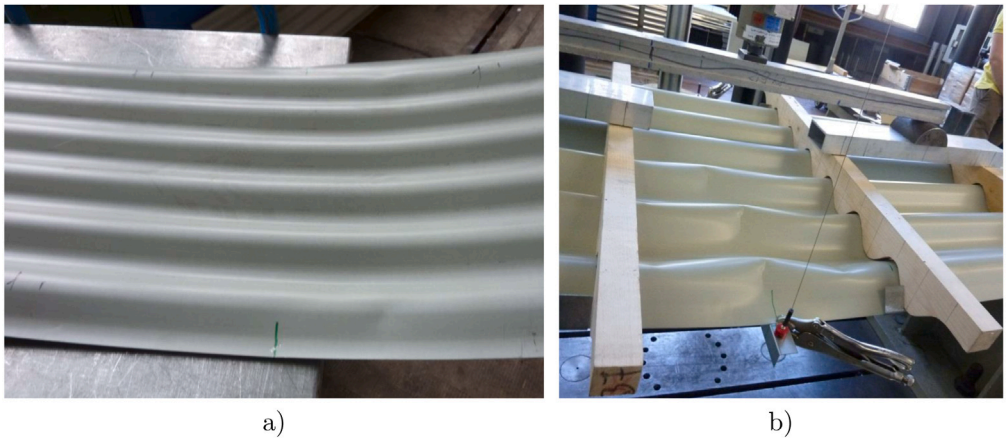

Fig. 13. Failure modes: (a) SSP-18-100-1 (yielding); (b) SSP-46-63-1 (buckling).

Table 6
Results of single span tests.

Test	Profile	t_{nom} [mm]	$t_{cor,obs}$ [mm]	$f_{yb,obs}$ [MPa]	F_{max} [kN]	F_m [kN]	$F_{u,k}$ [kN]	$M_{c,Rk,F}$ [kN m/m]
SSP-18-063–1					2.75			
SSP-18-063–2	Sin-18/76	0.63	0.523	333.7	2.69	2.753	2.617	1.09
SSP-18-063–3					2.82			
SSP-18-100–1					3.87			
SSP-18-100–2	Sin-18/76	1.00	0.943	402.0	3.91	3.890	3.697	2.08
SSP-18-100–3					3.89			
SSP-46-063–1					9.51			
SSP-46-063–2					9.03			
SSP-46-063–3	Sin-46/150	0.63	0.520	364.3	8.70	8.987	8.542	2.41
SSP-46-063–4					8.48			
SSP-46-063–5					9.17			
SSP-46-063–6					9.03			
SSP-46-100–1					13.57			
SSP-46-100–2	Sin-46/150	1.00	0.933	409.0	13.40	13.503	12.835	5.47
SSP-46-100–3					13.54			
				s	0.0258			
				k	1.92			

resistance of sinusoidal sheets. The results of the validation are presented in Table 7, where $M_{c,Rk,F}$ denotes bending moment resistance determined by the following methods:

Test	is the characteristic experimental resistance;
Elastic, exact	according to the conventional method with the exact second moment of area and elastic stress distribution;
Elastic, approx.	according to the conventional method with the approximated second moment of area and elastic stress distribution;
Plastic, exact	according to the conventional method with the exact second moment of area and plastic stress distribution;
StBK-N5	according to StBK-N5.

The values in brackets show the ratio of the corresponding value to the experimental (Test) value. The results show that the conventional method employing elastic stress distribution (Elastic, exact) leads to accurate predictions, although the resistance of Sin-46/150 with $t_{nom} = 0.63$ mm is found to be slightly unsafe. The conventional method with the approximated second moment of area according to EN 1993-4-1:2007 and elastic stress distribution (Elastic, approx.) provides sufficiently accurate and safe predictions for all the four considered profiles. The underestimation of bending resistance does not exceed 20%. In addition, StBK-N5 also provides accurate and safe prediction, which is less conservative than the conventional method. At the same time, the conventional method employing plastic stress distribution (Plastic, exact) leads to unsafe results in all cases and cannot be applied for the considered sinusoidal profiles.

From this point of view, both the conventional method and StBK-N5 demonstrated accurate and safe prediction of bending moment resistance of the sheets with the sinusoidal profile. The applicability range of the two methods is limited to the range of the tests conducted in this paper:

- the sheet is installed as a single span girder;
- the sheet is loaded only by uniformly distributed loads;
- the ratio R_ϕ/t is in the range $R_\phi/t \le 0.1E/f_{yb}$;
- the core thickness t_{cor} is in the range $t_{cor} \ge 0.55$ mm;
- the profile height d is in the range 18 mm $\le d \le$ 46 mm;
- the profile pitch l is in the range 76 mm $\le l \le$ 150 mm.

The reliability of the methods outside of the mentioned range can be further extended by additional experimental tests.

4.2. Internal support tests under downward loading

In all the internal support tests under downward loading, the failure occurred by buckling in crests, as depicted in Fig. 14. In all the tests, a non-linear load-bearing behavior was observed until the failure load was reached, as showed in Fig. 15a. In the figure, F_{max} indicates the failure load, i.e. the maximum load the specimen resists. Similar to the single span tests, the deviations between the values of the displacements F1 and F2 in the subcritical range (before reaching F_{max}) were negligible; therefore, the displacements F1 and F2 are shown by a common curve. The failure loads F_{max} for all the tests are listed in Table 8.

Unlike the single span tests, a test family for the internal support tests included all tests that allowed to develop an interaction curve, i.e. four tests. This procedure was chosen because the results in some of these test families were more scattered and this scatter would otherwise have had a negative effect on the other ones. At the same time, the k-factor was chosen for a sample size of $n \ge 10$, as the k-factor for $n = 4$ was found disproportionately conservative. The support reaction was determined as

$$R_{w,Rk,B} = F_{u,k}/b_v \tag{11}$$

The bending moment was calculated as

$$M_{c,Rk,B} = \frac{R_{w,Rk,B}L}{4} + \frac{qL_v(2L - L_v)}{8} \tag{12}$$

where $F_{u,k}$ is the characteristic load (including preload); L, L_v and b_v are the span, length and width of the sheet, respectively (Fig. 6); q is the self-weight of the sheet (Table 1). The characteristic values of support reactions $R_{w,Rk,B}$ and bending moments $M_{c,Rk,B}$ after statistical treatment are provided in Table 8.

The calculated characteristic support reactions and bending moments are then used to obtain the characteristic M/R-interaction of the sheets. A graphical M/R-interaction for Sin-46/150 with $t_{nom} = 0.63$ mm is presented in Fig. 16. The parameters of the M/R-interaction for all the tested sheets are summarized in Table 9 with the following notations:

$M_{c,Rk,F}$	is the span bending moment;
$M_{c,Rk,B}$ and R_1	are the maximum bending moment and its corresponding support reaction, respectively;
$R_{w,Rk,B}$ and M_2	are the maximum support reaction and its corresponding bending moment, respectively;
$M^0_{Rk,B}$ and $R^0_{Rk,B}$	are the interaction parameters.

As can be seen, the bending moment at the internal support is often considerably smaller than the bending moment in the span. Such behavior is explained by the fact that the linear load acts as a compressive force in the cross-section, reducing the moment capacity. The observed M/R-interaction demonstrates a dependence on the R_ϕ/t

Fig. 14. Failure mode, IS-46-10-100-60-2.

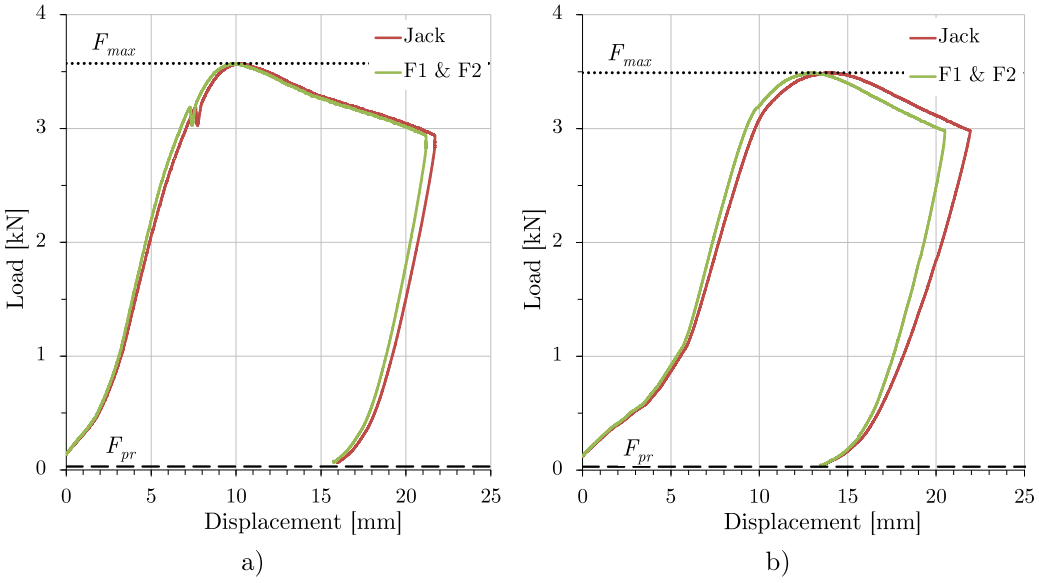

Fig. 15. Load–deflection curves: (a) IS-18-10-63-40-1; (b) IS-18-C-63-40-2.

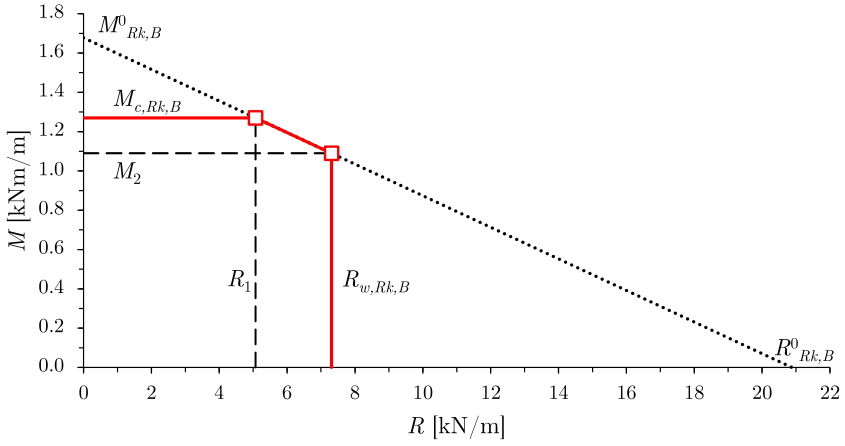

Fig. 16. M/R-interaction: Sin-46/150, $t_{nom} = 0.63$ mm.

Table 7
Validation of bending resistance.

Profile	t_{nom} [mm]	$t_{cor,obs}$ [mm]	f_{yb} [MPa]	$M_{c,Rk,F}$ [kN m/m]				
				Test	Elastic, exact	Elastic, approx.	Plastic, exact	StBK-N5
Sin-18/76	0.63	0.523	333.7	1.09	0.91(0.84)	0.82(0.75)	1.15(1.06)	0.88(0.80)
	1.00	0.943	402.0	2.08	1.98(0.95)	1.77(0.85)	2.50(1.20)	1.97(0.95)
Sin-46/150	0.63	0.520	364.3	2.41	2.41(1.00)	2.27(0.94)	3.14(1.30)	2.23(0.93)
	1.00	0.933	409.0	5.47	4.86(0.89)	4.56(0.83)	6.33(1.16)	4.73(0.86)

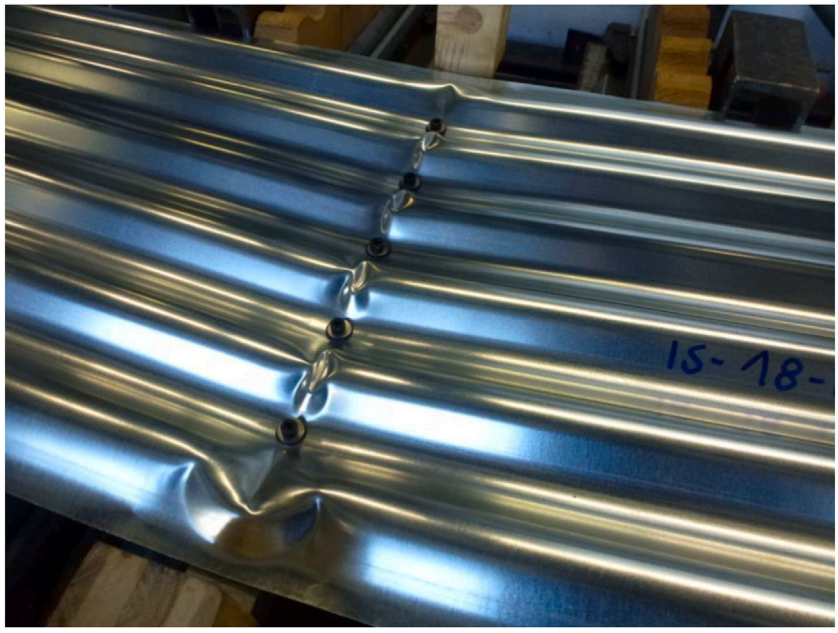

Fig. 17. Failure mode, IS-18-V-063-40-1 (buckling in the crest).

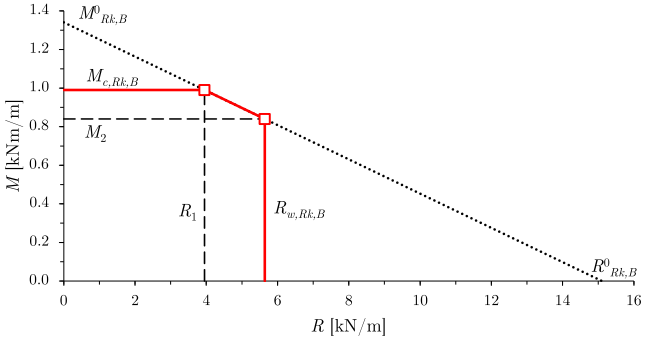

Fig. 18. M/R-interaction: Sin-46/150, $t_{nom} = 0.63$ mm, fixing in crests.

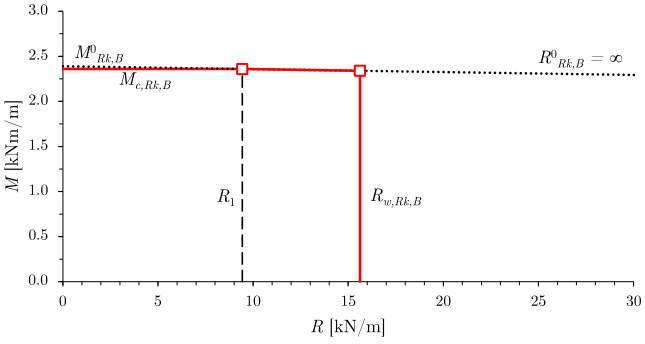

Fig. 19. M/R-interaction: Sin-46/150, $t_{nom} = 0.63$ mm, fixing in valleys.

ratio. For small R_ϕ/t ratios, the results show no reduction of the moment resistance in the span, e.g. Sin-18/76 with $t_{nom} = 1.00$ mm. For greater R_ϕ/t ratios, the bending moment at the internal support drops to a half of the bending moment capacity in the span, e.g. Sin-46/150 with $t_{nom} = 0.63$ mm. Another parameter that affects the bending moment capacity is the width of the support b_u: the reduction of the moment capacity at the support is greater for smaller support widths.

4.3. Internal support tests under upward loading

Similarly to downward loading, the sheets under upward loading failed by buckling in crests, as illustrated in Fig. 17. Similarly, the internal support tests demonstrated a non-linear behavior, as can be seen in Fig. 15b. The failure loads F_{max} for all the tests are listed in Table 10.

The statistical treatment was conducted similar to the internal support tests under downward loading. The characteristic support reactions and bending moments were determined in the same way as in the tests under downward loading, i.e. Eqs. (11), (12). The parameters of the characteristic M/R-combination for upward loading are summarized in Table 11, with the same notations that are used for downward loading. The results show that M/R-interaction strongly depends on the type of fixing. If the sheet is fixed in crests, M/R-interaction demonstrates a similar pattern as in the case with downward loading: the bending moment at the support considerably decreases in comparison with the bending moment in the span. Similarly, the interaction depends on the R_ϕ/t ratio, being particularly pronounced for greater R_ϕ/t ratios, e.g. Sin-46/150 with $t_{nom} = 0.63$ mm (Fig. 18). However, if the sheet is fixed in valleys (Fig. 19), the linear load is applied as a tension force in the cross-section, not reducing the bending moment

Table 8
Results of internal support tests, downward loading.

Test	Profile	t_{nom} [mm]	b_u [mm]	F_{max} [kN]	F_m [kN]	s	$F_{u,k}$ [kN]	$R_{w,Rk,B}$ [kN/m]	$M_{c,Rk,B}$ [kN m/m]
IS-18-10-063-40–1	Sin-18/76	0.63	10	3.57	3.58	0.0023	3.56	7.81	0.77
IS-18-10-063-40–2				3.58					
IS-18-10-063-80–1				2.01	2.02		2.01	4.40	0.88
IS-18-10-063-80–2				2.02					
IS-18-40-063-40–1	Sin-18/76	0.63	40	4.89	4.89	0.0064	4.83	10.58	1.05
IS-18-40-063-40–2				4.88					
IS-18-40-063-80–1				2.57	2.59		2.56	5.61	1.12
IS-18-40-063-80–2				2.61					
IS-18-10-100-40–1	Sin-18/76	1.00	10	9.32	9.23	0.0089	9.07	20.15	2.01
IS-18-10-100-40–2				9.14					
IS-18-10-100-100–1				4.17	4.15		4.08	9.06	2.27
IS-18-10-100-100–2				4.13					
IS-18-40-100-40–1	Sin-18/76	1.00	40	11.87	11.95	0.0054	11.82	25.88	2.58
IS-18-40-100-40–2				12.02					
IS-18-40-100-100–1				4.51	4.50		4.45	9.75	2.44
IS-18-40-100-100–2				4.49					
			k	1.92					
IS-46-10-063-60–1	Sin-46/150	0.63	10	5.95	5.94	0.0040	5.89	6.55	0.98
IS-46-10-063-60–2				5.93					
IS-46-10-063-100–1				4.32	4.34		4.31	4.79	1.20
IS-46-10-063-100–2				4.36					
IS-46-40-063-60–1	Sin-46/150	0.63	40	6.90	7.05	0.0347	6.58	7.31	1.09
IS-46-40-063-60–2				7.20					
IS-46-40-063-100–1				4.71	4.89		4.56	5.07	1.27
IS-46-40-063-100–2				5.07					
IS-46-10-100-60–1	Sin-46/150	1.00	10	18.08	18.25	0.0077	17.98	20.12	3.02
IS-46-10-100-60–2				18.42					
IS-46-10-100-120–1				11.29	11.28		11.11	12.43	3.74
IS-46-10-100-120–2				11.26					
IS-46-40-100-60–1	Sin-46/150	1.00	40	21.74	21.60	0.0058	21.36	22.40	3.36
IS-46-40-100-60–2				21.46					
IS-46-40-100-120–1				12.53	12.57		12.43	13.03	3.92
IS-46-40-100-120–2				12.60					
			k	1.92					

Table 9
Internal support tests, downward loading: characteristic M/R-interactions.

Profile	t_{nom} [mm]	R_ϕ/t	b_u [mm]	$M_{c,Rk,F}$ [kN m/m]	$M_{c,Rk,B}$ [kN m/m]	R_1 [kN/m]	M_2 [kN m/m]	$R_{w,Rk,B}$ [kN/m]	$M^0_{Rk,B}$ [kN m/m]	$R^0_{Rk,B}$ [kN/m]
Sin-18/76	0.63	36.5	10	1.09	0.88	4.40	0.77	7.81	1.02	32.00
			40		1.12	5.61	1.05	10.58	1.21	81.80
	1.00	23.0	10	2.08	2.27	9.06	2.01	20.15	2.49	104.44
			40		2.44	9.75	2.58	25.88	2.44	∞
Sin-46/150	0.63	47.6	10	2.41	1.20	4.79	0.98	6.55	1.81	14.26
			40		1.27	5.07	1.09	7.31	1.68	20.83
	1.00	30.0	10	5.47	3.74	12.43	3.02	20.12	4.92	52.04
			40		3.92	13.03	3.36	22.40	4.71	78.14

capacity. Therefore, the interaction parameter $R^0_{R,kB}$ tends to infinity and the bending moment resistance at the internal support is almost the same as the span resistance:

$$M_{c,Rk,B} \approx M_{c,Rk,F} \tag{13}$$

These results allow to conclude that the support reaction does not affect the bending moment under upward loading with fixing in valleys.

4.4. Discussion on M/R-interaction in internal support tests

This section compares the M/R-interaction of the two analyzed profiles (Sin-18/76 and Sin-46/150) of two thicknesses $t_{nom} = 0.63$ mm and 1.00 mm under downward and upward loading. Following the experimental program, the downward loading is considered with two support widths of $b_u = 40$ mm and $b_u = 10$ mm, while the upward loading is analyzed with fixing in crests and valleys. The comparative diagrams are presented in Figs. 20 and 21 with the following notations:

Downward, 40 mm	is downward loading with $b_u = 40$ mm support;
Downward, 10 mm	is downward loading with $b_u = 10$ mm support;
Upward, crest	is upward loading with fixing in crests;
Upward, valley	is upward loading with fixing in valleys.

As the reference value, the figures also plot the characteristic bending moment in span, i.e. the bending moment capacity without any reduction due to local deformations, which is denoted as “Span”. As can be seen from the diagrams, the reduction of the ultimate bending moment is influenced by the following parameters:

Table 10
Results of internal support tests, upward loading.

Test	Profile	t_{nom} [mm]	Fixing	F_{max} [kN]	F_m [kN]	s	$F_{u,k}$ [kN]	$R_{w,Rk,B}$ [kN/m]	$M_{c,Rk,B}$ [kN m/m]
IS-18-C-063-40–1	Sin-18/76	0.63	Crest	3.48	3.49	0.0084	3.42	7.52	0.74
IS-18-C-063-40–2				3.49					
IS-18-C-063-80–1				1.98	1.96		1.95	4.23	0.85
IS-18-C-063-80–2				1.94					
IS-18-V-063-40–1			Valley	5.41	5.35	0.0140	5.27	11.41	1.13
IS-18-V-063-40–2				5.28					
IS-18-V-063-80–1				2.52	2.49		2.45	5.31	1.06
IS-18-V-063-80–2				2.46					
IS-18-C-100-40–1	Sin-18/76	1.00	Crest	8.9	8.73	0.0165	8.62	18.83	1.87
IS-18-C-100-40–2				8.55					
IS-18-C-100-100–1				3.95	3.94		3.82	8.50	2.13
IS-18-C-100-100–2				3.93					
IS-18-V-100-40–1			Valley	10.87	10.97	0.0076	10.71	23.40	2.33
IS-18-V-100-40–2				11.06					
IS-18-V-100-100–1				4.24	4.23		4.18	9.02	2.26
IS-18-V-100-100–2				4.21					
			k	1.92					
IS-46-C-063-60–1	Sin-46/150	0.63	Crest	5.18	5.31	0.0222	4.96	5.64	0.84
IS-46-C-063-60–2				5.43					
IS-46-C-063-100–1				3.66	3.71		3.50	3.95	0.99
IS-46-C-063-100–2				3.76					
IS-46-V-063-60–1			Valley	14.17	14.36	0.0108	13.88	15.62	2.34
IS-46-V-063-60–2				14.55					
IS-46-V-063-100–1				8.66	8.67		8.48	9.43	2.36
IS-46-V-063-100–2				8.67					
IS-46-C-100-90–1	Sin-46/150	1.00	Crest	12.71	12.85	0.0282	12.02	13.67	3.08
IS-46-C-100-90–2				12.99					
IS-46-C-100-140–1				9.92	9.61		9.38	10.22	3.59
IS-46-C-100-140–2				9.29					
IS-46-V-100-90–1			Valley	21.96	22.21	0.0115	21.47	24.16	5.44
IS-46-V-100-90–2				22.45					
IS-46-V-100-140–1				14.84	14.71		14.51	16.01	5.62
IS-46-V-100-140–2				14.58					
			k	1.92					

Table 11
Internal support tests, upward loading: characteristic M/R-interaction.

Profile	t_{nom} [mm]	R_ϕ/t	Fixing type	$M_{c,Rk,F}$ [kN m/m]	$M_{c,Rk,B}$ [kN m/m]	R_1 [kN/m]	M_2 [kN m/m]	$R_{w,Rk,B}$ [kN/m]	$M^0_{Rk,B}$ [kN m/m]	$R^0_{Rk,B}$ [kN/m]
Sin-18/76	0.63	36.5	Crest	1.09	0.85	4.23	0.74	7.52	0.98	31.22
			Valley		1.06	5.31	1.13	11.41	1.06	∞
	1.00	23.0	Crest	2.08	2.13	8.50	1.87	18.83	2.34	94.17
			Valley		2.26	9.02	2.33	23.40	2.26	∞
Sin-46/150	0.63	47.6	Crest	2.41	0.99	3.95	0.84	5.64	1.34	15.16
			Valley		2.36	9.43	2.34	15.62	2.36	∞
	1.00	30.0	Crest	5.47	3.59	10.22	3.08	13.67	5.11	34.39
			Valley		5.62	16.01	5.44	24.16	5.62	∞

- R_ϕ/t ratio. The graphs show that Sin-18/76 with $t_{nom} = 1.00$ mm (the smallest R_ϕ/t ratio) is the least sensitive to the support reaction. On the other hand, Sin-46/150 with $t_{nom} = 0.63$ mm (the greatest R_ϕ/t ratio) demonstrates the most pronounced reduction of the bending moment capacity on the support.
- Pitch of the cross-section, i.e. the wave width l (see Fig. 3). The wave width represents the span length of the "bridge" that transmits local loads to the webs of the profile. From that point of view, the influence of the support reaction can be particularly pronounced for large pitches. Comparing the profiles with the same thicknesses, it can be noticed that Sin-46/150 has a considerably larger moment reduction than Sin-18/76.
- Support width b_u (for downward loading). Although the support width influences M/R-interaction, this influence is limited. The graphs demonstrate that the support width of 40 mm leads to a slightly smaller reduction than the support width of 10 mm.
- Fixing type (for upward loading). If the sheet is fixed in valleys, the support reaction acts as a tensile force in the cross-section, not affecting the bending moment. If the sheet is fixed in crests, the support reaction acts as a compressive force in the cross-section, significantly reducing the bending moment.

Unfortunately, the test campaign of this paper was not sufficient to propose any algebraic equation for the resistance of sinusoidal sheets at the internal support. Nevertheless, the paper presents valuable results that can be used for further research on this profile.

4.5. End support tests and shear tests

In all the end support tests, failure was caused by the deformation of the webs (web-crippling) at the end supports, followed by buckling of the sheets under the loading plate, as demonstrated in Fig. 22a. In

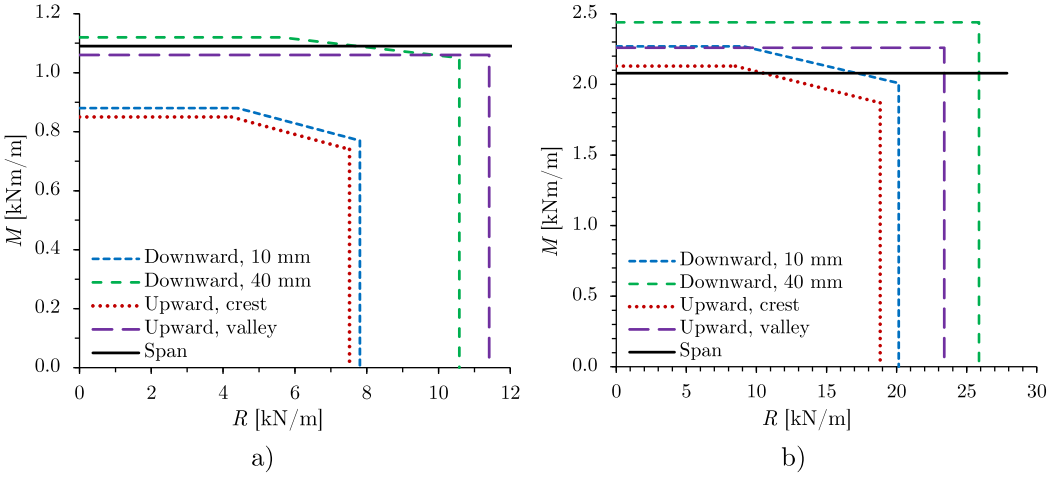

Fig. 20. M/R-interactions for Sin-18/76: (a) t_{nom} = 0.63 mm; (b) t_{nom} = 1.00 mm.

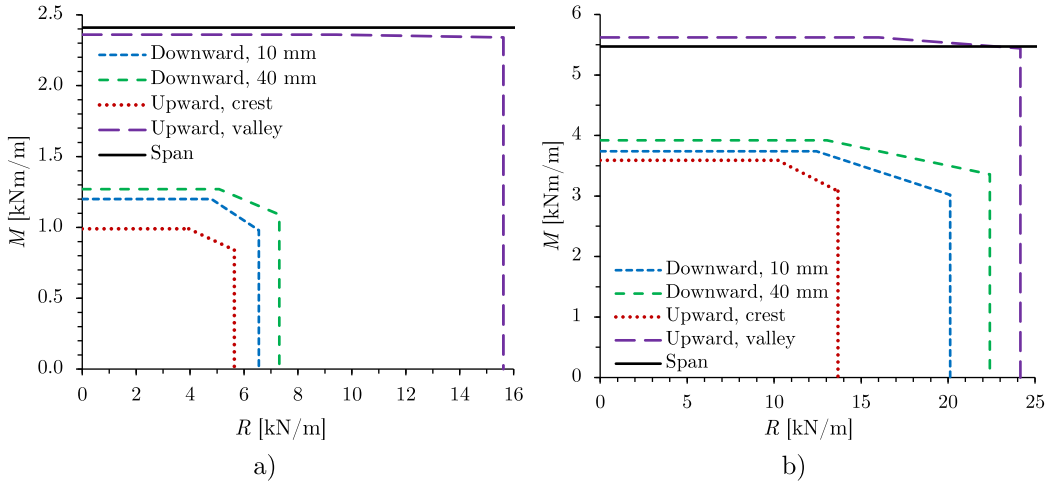

Fig. 21. M/R-interactions for Sin-46/150: (a) t_{nom} = 0.63 mm; (b) t_{nom} = 1.00 mm.

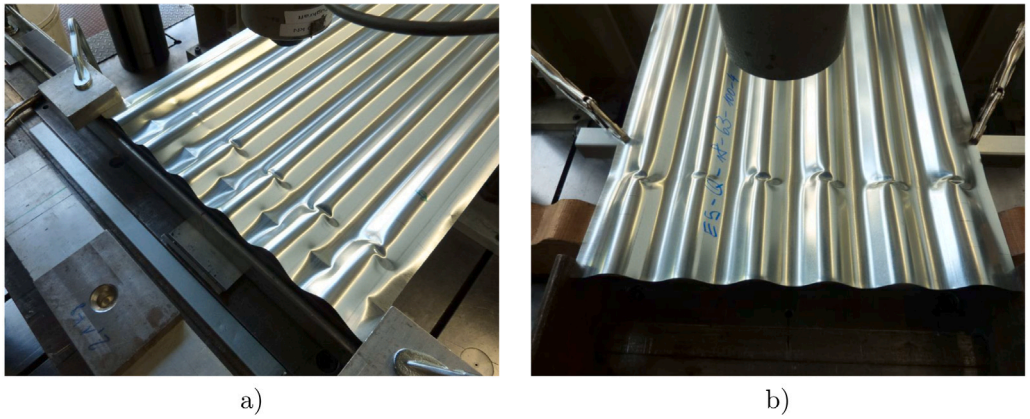

Fig. 22. Failure modes: (a) ES-Q-18-100-100-3; (b) ES-Q-18-063-100-1.

the test ES-Q-18-63-100-1 and both shear tests, failure occurred only by buckling in the zone with the maximum bending moment, as shown in Fig. 22b. In case of the shear tests, the applied load was limited by bending failure, and no shear failure at the support was achieved; therefore, the test results are lower than the estimated shear resistance. The applied load always exceeded the end support test results. Based on that, it can be concluded that the shear resistance is not the criterion that governs the strength of the profile.

The results of the end support tests are listed in Table 12, where F_{max} indicates the failure load, i.e. the maximum load the specimen resists. Based on the similarity of the conducted tests, all the end support and shear tests were combined into one test family, assuming that both profiles belong to the same population. The k-factor was

Table 12
Results of end support tests and shear tests.

Test	Profile	t_{nom} [mm]	F_{max} [kN]	F_m [kN]	$F_{u,k}$ [kN]	$R_{w,Rk,A}$ [kN/m]	$V_{w,Rk}$ [kN/m]
ES-Q-18-063-100–1			10.07				
ES-Q-18-063-100–2	Sin-18/76	0.63	9.81	9.84	9.19	18.13	–
ES-Q-18-063-100–3			9.63				
ES-Q-18-100-100–1			23.06				
ES-Q-18-100-100–2	Sin-18/76	1.00	22.05	21.75	20.31	40.09	–
ES-Q-18-100-100–3			20.14				
ES-Q-46-063-105–1			14.36				
ES-Q-46-063-105–2	Sin-46/150	0.63	14.65	14.91	13.92	13.26	–
ES-Q-46-063-105–3			15.71				
ES-Q-46-100-105–1			44.83				
ES-Q-46-100-105–2	Sin-46/150	1.00	43.40	44.07	41.16	39.20	–
ES-Q-46-100-105–3			43.97				
S-18-063-100–1	Sin-18/76	0.63	9.96	9.96	9.30	–	18.77
S-46-063-100–1	Sin-46/150	0.63	18.27	18.27	17.06	–	16.78
		s	0.0344				
		k	1.92				

chosen equal to 1.92, corresponding to a sample size of $n \geq 10$ (the actual number of the end support and shear tests is $n = 14$) with unknown V_x according to [1, Table A.2]. The support reaction $R_{w,Rk,A}$ and the characteristic shear force $V_{w,Rk}$ were determined by the same equation:

$$R_{w,Rk,A} = V_{w,Rk} = \frac{F_{u,k}(L-a)}{b_v L} \tag{14}$$

where $F_{u,k}$ is the characteristic load (including preload); L and b_v are the span and width of the sheet, respectively; a is the distance between the load and support axes (Fig. 9). The self-weight of the test specimens was neglected. The characteristic support reactions and shear forces after statistical treatment are summarized in Table 12.

Unfortunately, the test campaign of this paper was not sufficient to propose any algebraic equation for the end support resistance of sinusoidal sheets. Nevertheless, the presented results can be used for further research on this profile.

5. Conclusions

The paper presents the results of the research on the corrugated sheets with the sinusoidal profile. Three types of tests were conducted in the study, including single span tests, internal supports tests and end support tests.

The single span tests were conducted to obtain the characteristic moment resistance of the sheets. The majority of the analyzed sheets failed by local buckling of crests in the middle of the span. However, for the sheets with the smallest height and the largest thickness buckling was prevented; and these sheets failed by yielding, developing plastic deformation along the whole span of the sheets. The results of the single span tests were used to analyze the applicability of the existing design methods for the bending resistance of sinusoidal sheets, such as the conventional method and the Swedish code StBK-N5. Both methods demonstrated accurate and safe prediction of bending moment resistance of the analyzed sheets. In addition, the approximated solution of EN 1993-4-1:2007 for the section properties of the sinusoidal sheets was found to be safe, leading to a slightly more conservative prediction than the exact equation from the Strength of Materials. The two validated approaches can be recommended as simple and reliable methods to calculate the load-bearing capacity of sinusoidal sheets within the validity range considered in the paper. Additional research supported by experimental studies can extend the methods to sheets with different geometry.

Attention was also paid to the internal support tests to investigate the interaction between the moment resistance and the support reaction. The conducted tests showed that the interaction strongly depends on the direction of the applied load and the type of sheet fixing. In case of downward loading or upward loading with fixing in the crest, the bending moment at the internal support was often considerably smaller than the bending moment in the span. The observed M/R-interaction depended on the R_ϕ/t ratio, being particularly strong for large R_ϕ/t ratios. Another parameter that affected the bending moment capacity at the support was the width of the support. In case of upward loading with fixing in valleys, the support reaction demonstrated no influence on the bending moment and the bending moment resistance at the internal support was almost the same as the resistance in the span.

The end support tests allowed to determine the end support resistance of the sheets; however, the amount of the tests was not sufficient to establish any general equation. The shear tests showed that the shear resistance is not the criterion that governs the strength of the profile, as it exceeded the end support reaction in all the conducted tests. Although the test campaign of this paper was not sufficient to propose algebraic equations for the resistance of sinusoidal sheets at the internal and end supports, the presented results can be used for further research on this profile, especially for the validation of developed FE models. In addition, as the tested profiles are current representatives in the building market, the conducted research may be also valuable for engineers, providing them the strength values of sinusoidal profiles at the intermediate and end supports.

CRediT authorship contribution statement

Marsel Garifullin: Writing - original draft, Writing - review & editing. **Kristo Mela:** Writing - review & editing. **Thibault Renaux:** Conception and design of study, Analysis and/or interpretation of data. **David Izabel:** Conception and design of study, Analysis and/or interpretation of data, Writing - original draft, Writing - review & editing. **Rainer Holz:** Conception and design of study, Analysis and/or interpretation of data. **Christian Fauth:** Conception and design of study, Acquisition of data, Analysis and/or interpretation of data, Writing - review & editing.

Declaration of competing interest

The authors declare that they have no known competing financial interests or personal relationships that could have appeared to influence the work reported in this paper.

Acknowledgments

This presented study was funded by the Research Fund for Coal and Steel (RFCS) under the grant agreement No. 75 4092. All authors approved the version of the manuscript to be published.

References

[1] CEN, Eurocode 3: Design of steel structures – Part 1-3: General rules. Supplementary rules for cold-formed members and sheeting (EN 1993-1-3:2006). Brussels, 2006.

[2] H.L. Wakeland, Flexural properties of corrugated metal roofing, 1954.

[3] R.L. Cary, Inelastic flexural stability of corrugations, in: W.-W. Yu, J.H. Senne (Eds.), Eighth International Specialty Conference on Cold-Formed Steel Structures, University of Missouri Rolla, St. Louis, Missouri, 1986, pp. 509–522.

[4] D. Briassoulis, Equivalent orthotropic properties of corrugated sheets, Comput. Struct. 23 (1986) 129–138.

[5] R.A. Shimansky, M.M. Lele, Transverse stiffness of a sinusoidally corrugated plate, Mech. Struct. Mach. 23 (1995) 439–451.

[6] K. Liew, L. Peng, S. Kitipornchai, Buckling analysis of corrugated plates using a mesh-free Galerkin method based on the first-order shear deformation theory, Comput. Mech. 38 (2006) 61–75.

[7] K.M. Liew, L.X. Peng, S. Kitipornchai, Nonlinear analysis of corrugated plates using a FSDT and a meshfree method, Comput. Methods Appl. Mech. Engrg. 196 (2007) 2358–2376.

[8] Y. Xia, M.I. Friswell, E.I. Flores, Equivalent models of corrugated panels, Int. J. Solids Struct. 49 (2012) 1453–1462.

[9] Z. Ye, V.L. Berdichevsky, W. Yu, An equivalent classical plate model of corrugated structures, Int. J. Solids Struct. 51 (2014) 2073–2083.

[10] K.J. Park, K. Jung, Y.W. Kim, Evaluation of homogenized effective properties for corrugated composite panels, Compos. Struct. 140 (2016) 644–654.

[11] D.J. Henderson, J.D. Ginger, Response of pierced fixed corrugated steel roofing systems subjected to wind loads, Eng. Struct. 33 (12) (2011) 3290–3298.

[12] T. Nordstrand, L.A. Carlsson, H.G. Allen, Transverse shear stiffness of structural core sandwich, Compos. Struct. 27 (1994) 317–329.

[13] G. Bartolozzi, M. Pierini, U. Orrenius, N. Baldanzini, An equivalent material formulation for sinusoidal corrugated cores of structural sandwich panels, Compos. Struct. 100 (2013) 173–185.

[14] C. Dou, Z.Q. Jiang, Y.L. Pi, Y.L. Guo, Elastic shear buckling of sinusoidally corrugated steel plate shear wall, Eng. Struct. 121 (2016) 136–146.

[15] J.Z. Tong, Y.L. Guo, Shear resistance of stiffened steel corrugated shear walls, Thin-Walled Struct. 127 (2018) 76–89.

[16] Q. Cao, J. Huang, Experimental study and numerical simulation of corrugated steel plate shear walls subjected to cyclic loads, Thin-Walled Struct. 127 (2018) 306–317.

[17] L.A. Fülöp, D. Dubina, Performance of wall-stud cold-formed shear panels under monotonic and cyclic loading - Part I: Experimental research, Thin-Walled Struct. 42 (2004) 321–338.

[18] C. Dou, Y.L. Pi, W. Gao, Shear resistance and post-buckling behavior of corrugated panels in steel plate shear walls, Thin-Walled Struct. 131 (2018) 816–826.

[19] G. Correia Lopes, C. Couto, P. Vila Real, N. Lopes, Elastic critical moment of beams with sinusoidally corrugated webs, J. Construct. Steel Res. 129 (2017) 185–194.

[20] R.J. Pimenta, G. Queiroz, S.M. Diniz, Reliability-based design recommendations for sinusoidal-web beams subjected to lateral–torsional buckling, Eng. Struct. 84 (2015) 195–206.

[21] J.P.S. de Oliveira, A.F.G. Calenzani, R.H. Fakury, W.G. Ferreira, Elastic critical moment of continuous composite beams with a sinusoidal-web steel profile for lateral–torsional buckling, Eng. Struct. 113 (2016) 121–132.

[22] A. Piekarczuk, P. Więch, K. Malowany, Numerical investigation into plastic hinge formation in arched corrugated thin-walled profiles, Thin-Walled Struct. 119 (2017) 13–21.

[23] J.M. Davies, C. Jiang, Design procedures for profiled metal sheeting and decking, Thin-Walled Struct. 27 (1) (1997) 43–53.

[24] A. Biegus, D. Czepizak, Research on the interactive resistance of corrugated sheets under combined bending and contact pressure, Thin-Walled Struct. 44 (8) (2006) 825–831.

[25] K. Le Tran, L. Davaine, C. Douthe, K. Sab, Stability of curved panels under uniform axial compression, J. Construct. Steel Res. 69 (2012) 30–38.

[26] CEN, Eurocode 3 - Design of steel structures - Part 4-1: Silos (EN 1993-4-1:2007), 2007.

[27] StBK-N5, Tunnplåtsnormen [Swedish Code for Light-Gauge Metal Structures], Stalbyggnadsinstitutet, Stockholm, 1979.

[28] CEN, Continuously hot-dip coated steel flat products for cold forming – Technical delivery conditions (EN 10346:2015), 2015.

[29] CEN, Metallic materials – Tensile testing – Part 1: Method of test at room temperature (ISO 6892-1:2016), 2016.

[30] Avis Techniques, E-Cahier du CSTB 3730. Cahier des Prescriptions Techniques Communes aux Procédés de Planchers Collaborants [Common Technical Specifications for Composite Flooring Processes], CSTB, 2014, [in French].